Chemical Science

ROYAL SOCIETY OF CHEMISTRY

EDGE ARTICLE

View Article Online
View Journal | View Issue

Cite this: *Chem. Sci.*, 2023, **14**, 113

All publication charges for this article have been paid for by the Royal Society of Chemistry

Received 31st August 2022
Accepted 16th September 2022

DOI: 10.1039/d2sc04862k

rsc.li/chemical-science

Ultrabright AIEdots with tunable narrow emission for multiplexed fluorescence imaging†

Xiaobo Zhou,‡* Lingfeng Zhao,‡ Ke Zhang, Chaojie Yang, Shijie Li, Xiaoxia Kang, Guo Li, Qi Wang, Haiwei Ji, Mingmin Wu, Jinxia Liu, Yuling Qin* and Li Wu*

AIEgen doped fluorescent nanodots (AIEdots) have attracted lots of attention, due to their superior characteristics as fluorescent probes, such as excellent photostability, large Stokes shift, high brightness and tunable emission. Unfortunately, most of the currently available AIEdots exhibit broad emission bandwidth, which limits their applications in multiplexed fluorescence imaging and detection. In this work, the strategy of designing and fabricating narrow emissive AIEdots (NE-AIEdots) with tunable wavelengths was presented by constructing a light-harvesting system with high energy transfer efficiency. Efficient intra-particle energy transfer from highly doped AIEgens, serving as the light-harvesting antenna, to the lightly doped narrow emissive fluorophore, resulted in high brightness and narrow emission. The emission band of NE-AIEdots with the full-width-at-half-maximum varied from 18 to 36 nm was 3–6.3 times narrower than that of traditional AIEdots. The single-particle brightness of NE-AIEdots was over 5-times that of commercial quantum dots under the same excitation and collection conditions. Taking advantage of the superior performance of these NE-AIEdots, multiplexed fluorescence imaging of lymph nodes in living mice was realized, which supported the future applications of NE-AIEdots for *in vivo* multiplexed labeling and clinical surgery.

Introduction

Fluorescent probes have been widely applied for biomedical applications, such as fluorescence microscopy imaging, flow cytometry, surgery navigation, and immunofluorescence analysis.[1–4] Up to now, a variety of luminescent materials have been developed and applied as fluorescent probes.[5–10] Among them, organic dyes are the most commonly used fluorescent probes, which is attributed to their high quantum yield, tunable emission, small size, modifiable structure, and identical single-molecule optical properties.[11–14] Although promising, the brightness of a single dye is far below that of single luminescent nanomaterials such as QDs (quantum dots), LnNCs (lanthanide nanocrystals), and Pdots (polymer dots), which is attributed to the limited photon absorption capacity of dyes.[15,16] This results in a low signal-to-noise ratio in fluorescence imaging. Developing organic dye-doped nanoparticles (ODNPs) has been proven to be an efficient strategy for designing brighter fluorescent probes, which both maintains the fluorescence properties and improves the photostability of the dyes. Enhanced single-fluorophore brightness can be successfully achieved in this way by increasing the number of dyes in a single nanoparticle.[17–20] However, the bottleneck of the proposed method is the limited ratio (~0.5%) of the doped dyes in ODNPs, which is extremely restricted by the severe fluorescence quenching effect of most organic dyes at the aggregation state. Although further enhanced brightness of ODNPs can be achieved by introducing a functional group to enlarge the distance between the dyes or increasing the size of nanoparticles,[21–24] there remains a limitation in brightness enhancement.

AIEgens are a kind of organic fluorogen with aggregation-induced emission characteristics, which display strong fluorescence at aggregation states or solid states.[13,25] This unique property makes AIEgens promising candidates for constructing highly emissive nanofluorophores with high doping contents of luminescent centers. Recently, AIEgen doped fluorescent nanodots (AIEdots) have aroused great interest because of their ultra-small size, high brightness, large Stokes shift, and excellent photostability.[26–28] Despite their obvious advantages and significant developments, the drawback that limits the broad application of AIEdots in biomedicine research, especially for multiplexed fluorescence analysis, is their broad emission band.[29–36] Therefore, there is a high demand to develop efficient strategies to narrow the emission band of AIEdots.

Herein, a series of wavelength-tunable AIEdots with narrow emission bands and enhanced brightness have been developed for multiplexed fluorescence imaging *in vitro* and *in vivo*. Inspired by the light-harvesting strategies of constructing bright

School of Public Health, Nantong University, Nantong 226019, Jiangsu, China. E-mail: wuli8686@ntu.edu.cn; xbzhou@ntu.edu.cn; ylqin@ntu.edu.cn

† Electronic supplementary information (ESI) available. See DOI: https://doi.org/10.1039/d2sc04862k

‡ These authors contributed equally to this work.

and functional supramolecular systems and Pdots,[28,37–40] which confirmed that efficient energy transfer from donors to acceptors could dramatically annihilate the emission of donors and amplify the emission of acceptors, we hope to demonstrate an effective strategy to construct narrow emissive AIEdots (NE-AIEdots) by using AIEgens as the donor and light-harvesting antenna, and narrow emissive organic dye as the acceptor and emitter (Scheme 1). Taking advantage of the broad emission of the donor AIEgens and the tunable emission wavelength of both the donor and acceptor, varied NE-AIEdots with tunable excitation and emission can be designed. In such a light-harvesting system, the common aggregation caused quenching (ACQ) effect of organic dyes in ODNPs can be extremely reduced by lightly doping the dyes in AIEdots while maintaining the high brightness and narrowing the emission band of AIEdots by efficient energy transfer from AIEgens to narrow emissive organic dyes. In the prepared NE-AIEdots, the component proportions of AIEgens and organic dyes are 80% and 0.36–0.87%, respectively. The efficiencies of energy transfer from AIEgens to narrow emissive dyes are above 90% in these light-harvesting systems with a donor to acceptor molar ratio of over 200/1. According to this strategy, the prepared multicolor NE-AIEdots exhibit a large extinction coefficient over 16 L g^{-1} cm^{-1}, high quantum yield over 70% in water, narrow emission band with full-width-at-half-maximum (FWHM) of 36 nm, tunable emission peak ranging from 560 nm to 790 nm and large Stokes shift over 300 nm. To the best of our knowledge, the FWHM of NE-AIEdots fabricated in this work are currently the narrowest among the reported AIEdots corresponding to different emission wavelengths. Additionally, as single nanofluorophores, the prepared NE-AIEdots are about 5.2 times brighter than commercial quantum dots QD525. Such NE-AIEdots with a narrow emission band, high brightness, and large Stokes shifts show obvious advantages for multiplexed biological imaging *in vitro* and *in vivo*. Significantly, the strategy presented here provided a general approach to the design and construction of NE-AIEdots for multiplexed biological detection.

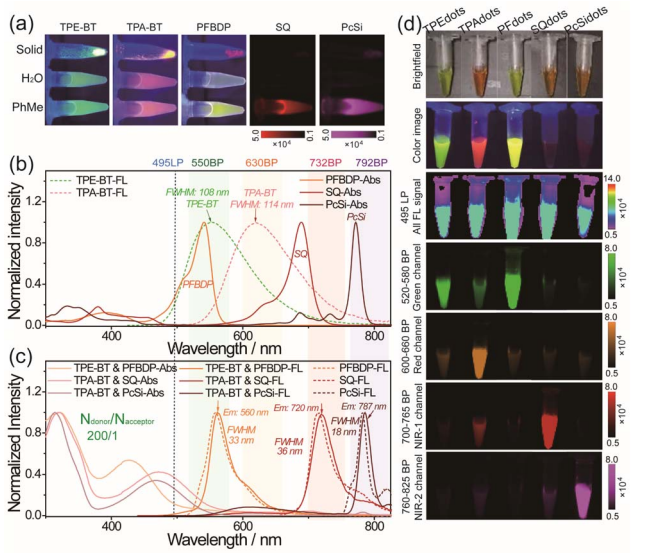

Fig. 1 (a) Photos and fluorescence images of different fluorophores in toluene (PhMe) and water and at a solid-state under the excitation of 365 nm UV lamp (TPE-BT, TPA-BT and PFBDP) and 630 nm LED light source (SQ and PcSi), respectively. (b) UV-vis absorption spectra of PFBDP, SQ and PcSi, and fluorescence spectra of TPE-BT and TPA-BT. (c) UV-Vis absorption spectra and fluorescence spectra of PFdots, SQdots and PcSidots, and fluorescence spectra of PFBDP, SQ and PcSi. (d) Images of TPEdots, TPAdots, PFdots, SQdots and PcSidots under different conditions. Brightfield: photos taken under room light. Color image: photos were taken under the excitation of UV light (365 nm). Fluorescence images taken under the excitation of a 450 nm LED light source with different collection channels. All FL signals: 495 nm long-pass filter (495LP); green channel: 520–580 nm bandpass filter (550BP); red channel: 630BP; NIR-1 channel: 732BP; NIR-2 channel: 792 BP.

Results and discussion

Design, preparation, and characterization of NE-AIEdots

The two kinds of AIEgens TPE-BT and TPA-BT, and three kinds of organic dyes PFBDP, SQ, and PcSi were synthesized according to the previous literature (Scheme S1†).[41–44] The chemical structures of these are illustrated in Scheme 1. The photophysical properties of the as-synthesized AIEgens and narrow emissive dyes were first studied (Fig. 1, S1–S5 and Table S1†). As shown in Fig. 1a, TPE-BT and TPA-BT exhibited remarkable strong fluorescence in the organic solvent, water, and solid state. However, significantly attenuated fluorescence signals of the above obtained three organic dyes were observed in water and at a solid-state compared to those dispersed in the organic solvent. In addition, in the mixture of THF/water with different water fractions (f_w), both TPE-BT and TPA-BT showed decreased and bathochromically shifted emission with the gradual addition of water into THF ($f_w \leq 50$ vol%). When the proportion of the added water was further increased ($f_w \geq 50$ vol%), their emission was dramatically enhanced with an increase in f_w (Fig. S1f and S1g†). Moreover, TPE-BT and TPA-BT exhibit gradually decreased and bathochromically shifted emission performance with increased solvent polarity (Fig. S1h–k†), indicating that TPE-BT and TPA-BT undergo the twisted intramolecular charge transfer (TICT) process in the THF/water mixture with the low water fraction and show an obvious AIE effect in the mixture with the high water fraction.[45,46] These results confirmed that TPE-BT and TPA-BT showed a characteristic AIE feature, while PFBDP, SQ, and PcSi showed the typical ACQ performance, which is in accordance with many previous studies.[26,47–50] The absorption and emission spectra of AIEgens and organic dyes are shown in Fig. 1b. According to the considerable overlap between the absorption band of organic dyes and the emission band of AIEgens, the Förster radius (R_0) of the different donor–acceptor pairs was calculated to be 4.56 nm (TPE-BT&PFBDP), 5.24 nm (TPE-BT&SQ), 4.42 nm (TPE-BT&PcSi), 3.57 nm (TPA-BT&PFBDP), 7.04 nm (TPA-BT&SQ) and 6.02 nm (TPA-BT&PcSi), respectively.[20–23,51] Therefore, an efficient energy transfer from bright emissive AIEgens to the corresponding narrow emissive organic dyes could take place when they were close enough to each other (Scheme 1).

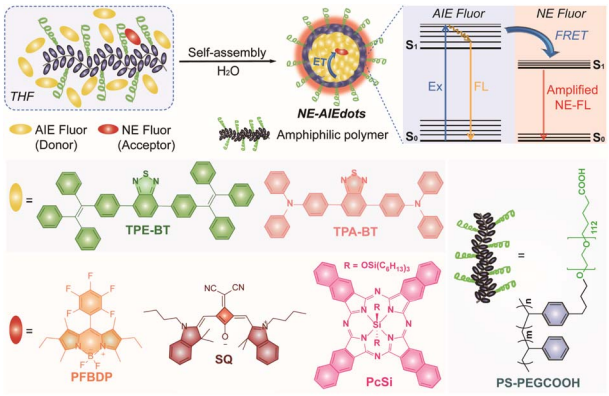

Scheme 1 Schematic illustration of the design and preparation of NE-AIEdots and the chemical structure of the doped AIEgens and organic dyes.

The AIEdots with surface carboxyl groups were prepared through the nanoprecipitation method by using amphiphilic polymer PS-PEGCOOH as the encapsulation medium (Scheme 1). To further optimize the brightness of NE-AIEdots, dual fluorophore co-doped nanodots were prepared with a high mass fraction (80%) of AIEgens and different molar percentages ($N_{AIEgens}/N_{dyes}$ ratio ranged from 2000/1 to 10/1) of organic dyes. For the nanodots with a low doping ratio of organic dyes ($N_{AIEgens}/N_{dyes}$ > 200/1), significantly enhanced narrow emission with the increasing molar percentages of the dyes was observed (Fig. S6–S10†). Instead, the high doping ratio of organic dyes in nanodots resulted in the obvious attenuation of emission, which suggests the ACQ effect of organic dyes (Fig. S11a–f†). Specifically, highly efficient energy transfer (up to 90%) from AIEgens to narrow emissive dyes could be achieved by blending TPE-BT&PFBDP, TPA-BT&SQ, or TPA-BT&PcSi with a small number of acceptors (below 1.0%, Fig. S11g–i†). The Stern–Volmer quenching constants of different donor–acceptor pairs were calculated to be 934.1 (TPE-BT&PFBDP), 7455.4 (TPA-BT&SQ), and 2265.7 (TPA-BD&PcSi), respectively, which indicated that one PFBPD molecule could potentially quench 934 TPE-BT molecules, one SQ molecule could potentially quench 7455 TPA-BT molecules and one PcSi molecule could potentially quench 2265 TPA-BT molecules in the organic nanodots, confirming the amplified energy transfer from AIEgens to narrow emissive dyes (Fig. S11j–l†). Based on the above optimizations, a series of narrow emissive AIEdots with brightness and wavelength-tunable fluorescence were obtained (Fig. 1c). According to the name of the luminescent center which dominates the emission of nanodots, the fluorescent dots were named TPEdots (consisting of TPE-BT and PS-PEGCOOH), TPAdots (consisting of TPA-BT and PS-PEGCOOH), PFdots (consisting of TPE-BT, PFBDP, and PS-PEGCOOH, N_{TPE-BT}/N_{PFBDP} is 100/1), SQdots (consisting of TPA-BT, SQ, and PS-PEGCOOH and N_{TPA-BT}/N_{SQ} is 200/1), PcSidots (consisting of TPA-BT, PcSi, and PS-PEGCOOH and N_{TPA-BT}/N_{PcSi} is 200/1), respectively.

The photophysical properties of these AIEdots were determined first (Fig. S12, S13, and Table S2†). Compared to the broad emission bandwidth of TPEdots (FWHM ~ 108 nm) and TPAdots (FWHM ~ 114 nm), obvious narrow emissions of PFdots (FWHM ~ 33 nm), SQdots (FWHM ~ 36 nm), and PcSidots (FWHM ~ 18 nm) allowed multiplexed fluorescence imaging in more channels. Compared to the above-designed PFdots, SQdots, and PcSidots, the organic solutions (toluene) containing identical amounts of AIEgens, narrow emissive dyes, and PS-PEGCOOH showed only strong broad emission from AIEgens while not narrow emission from dyes (Fig. S14 and S15†). Additionally, the above mixtures retained almost the same fluorescence intensity as equivalent AIEgens themselves dispersed in the same organic solvent. These results indicated that a negligible internal filtration effect was generated in such mixed and co-doped systems. According to the excitation spectra of the NE-AIEdots, AIEgens, narrow emissive dyes, and the simple mixtures of AIEgens, dyes, and PS-PEGCOOH (Fig. S16†), NE-AIEdots showed similar excitation spectra to those of TPEdots and TPAdots. Furthermore, the optical properties (emission band, intensity, and lifetime) of the mixtures, consisting of AIEdots and narrow emissive dye-doped organic nanoparticles dispersed in water, were similar to those of the corresponding AIEdots. In comparison, the NE-AIEdots had almost the same lifetime, emission band, and fluorescence decay curves as the corresponding narrow emissive dye-doped nanoparticles (Fig. S17–S20†). Additionally, the fluorescence lifetime of the doped AIEgens in nanodots decreased when the energy transfer acceptor (narrow emissive dyes) was co-doped. These results further suggested that highly efficient energy transfer from centuple AIEgens to narrow emissive dyes was realized based on such a facilely prepared co-doping nanosystem. As shown in Fig. 1d, the fluorescence signal intensity of NE-AIEdots showed a more distinct difference in various optical signal collection channels than that of TPEdots and TPAdots. In addition, the as-prepared NE-AIEdots demonstrated high stability over two weeks of storage (Fig. S21a and b†). To ensure the optical performance of the constructed NE AIEdots in future biological applications, the leakage test of the NE-AIEdots in different media including PBS solutions (100 mM phosphate buffer solutions), SBF (simulated body fluid) solutions, FBS solutions (FBS containing PBS solutions, 10 vol%) and cell culture medium RMPI-1640 was performed by monitoring the fluorescence intensity of the narrow emission band, as well as the diameter of the as-obtained NE AIEdots. As a result, no significant differences were observed for both the diameter and the fluorescence intensity of the tested NE-AIEdots when measured in different media for 72 h (Fig. S21c–h†). These results indicate that the leakage issue of these prepared NE-AIEdots under our experimental conditions is negligible. As confirmed by the DLS and TEM results (Fig. 2a–j), all of the above obtained AIEdots exhibited small size (~30 nm) and uniform morphology. The superior optical performance of NE-AIEdots made them promising candidates for multiplexed fluorescence bioimaging.

When using fluorophores as indicating labels in a biological system, the brightness of a single fluorophore is a crucial factor that affects the accuracy and sensitivity of biosensing and bio-

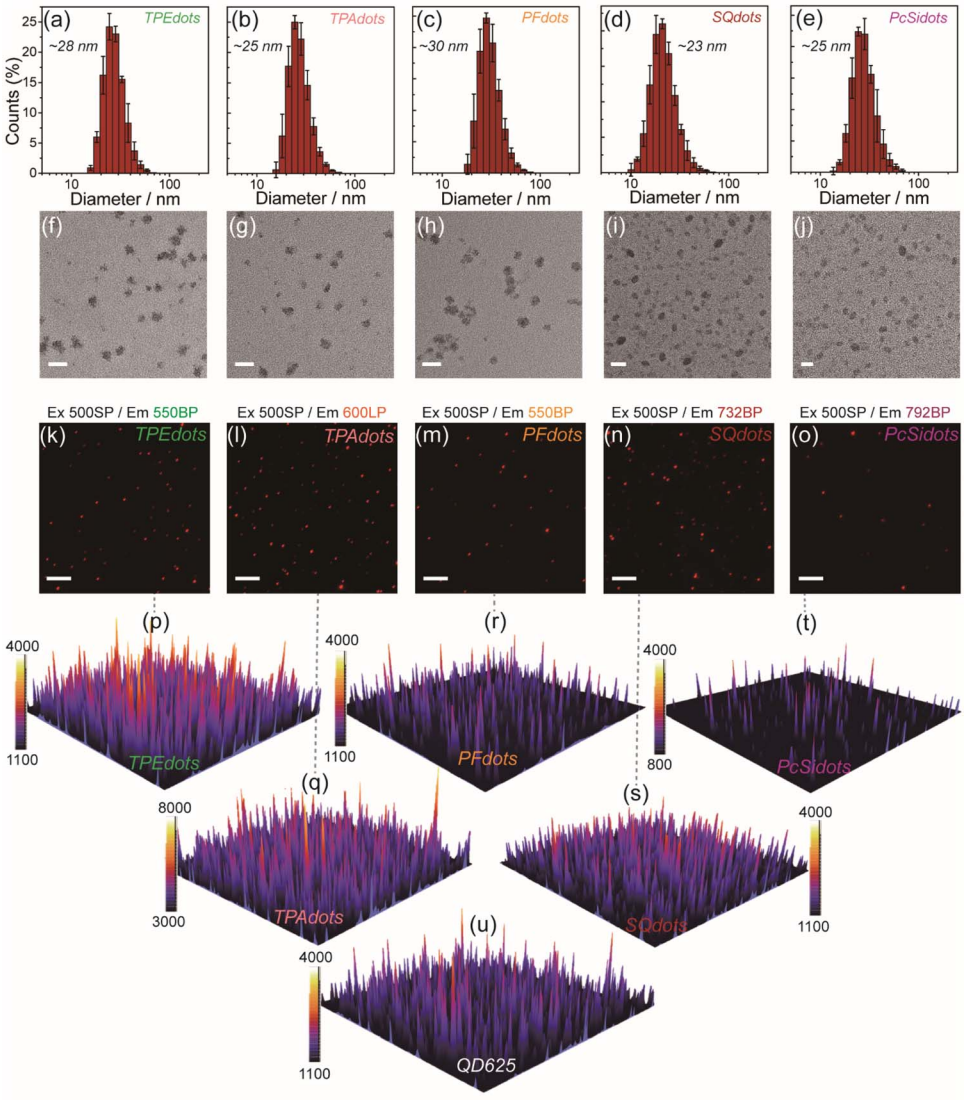

Fig. 2 Histograms of size distribution measured by DLS for (a) TPEdots, (b) TPAdots, (c) PFdots, (d) SQdots and (e) PcSidots. TEM images of (f) TPEdots, (g) TPAdots, (h) PFdots, (i) SQdots and (j) PcSidots. Scale bar: 50 nm. Single-particle fluorescence images of (k) TPEdots, (l) TPAdots, (m) PFdots, (n) SQdots and (o) PcSidots obtained with the excitation of a xenon lamp using the same excitation filter (500SP) and different emission filters (550BP, 600LP, 550BP, 732BP and 792BP). Scale bar: 5 μm. 3D representations of the corresponding fluorescence images of (p) TPEdots, (q) TPAdots, (r) PFdots, (s) SQdots and (t) PcSidots in comparison to that of (u) QD625 (Ex-500SP and Em-600LP).

detection. A single-particle imaging test was designed and performed to determine the brightness of the obtained TPEdots, TPAdots, PFdots, Sqdots, and PcSidots. Under the same collection (495LP and 600 LP) and excitation conditions (405 nm bandpass filter and 500 nm short-pass filter, 405BP and 500SP), the single-particle brightness of these AIEdots was separately measured by using commercial Qdots as the reference (QD525 and QD625, Fig. S22†). Under the test conditions described above, the measured average fluorescence intensity per particle of TPEdots and PFdots is 4.0 times and 5.2 times higher than that of QD525, respectively. The brightness of TPAdots, Sqdots, and PcSidots is 2.0 times, 1.02 times, and 0.43 times that of QD625, respectively (Fig. S23–S25†). As shown in Fig. 2k–o, single-particle imaging of the prepared AIEdots was further estimated by using the same excitation conditions (500 nm short-pass filter, 500SP) and the same image acquiring conditions but different collecting emission signals with different bandpass filters (550BP, 630BP, 732BP, and 792BP). In comparison, the above-obtained AIEdots still exhibited comparative single-particle brightness to that of QD625 (Fig. 2p–u). In conclusion, the excellent optical properties of the prepared NE-AIEdots guaranteed their further applications in multiplexed labeling and imaging.

NE-AIEdots for multiplexed fluorescence imaging *in vitro* and *in vivo*

Before the further application of these multicolor NE-AIEdots for fluorescence imaging in living biological systems, the

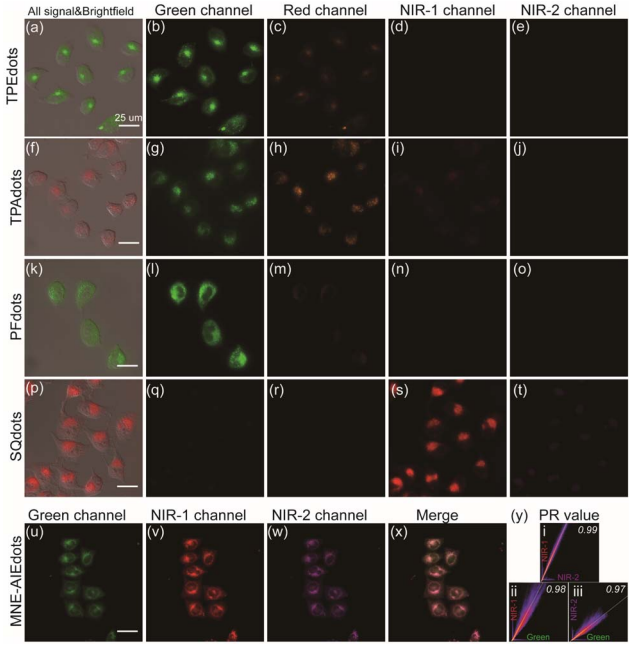

Fig. 3 Fluorescence images of cells incubated with the prepared AIEdots (20 μg mL^{-1}) for 24 h under different signal collection conditions. (a–e) TPEdots, (f–j) TPAdots, (k–o) PFdots and (p–t) SQdots. An excitation: xenon lamp equipped with a 500SP filter. Signal collection conditions: green channel-550BP, red channel-630BP, NIR-1 channel-732BP, NIR-2 channel-792BP. (u–x) Fluorescence images of cells incubated for 24 h with MNE-AIEdots under different signal collection conditions. Scale bar: 25 μm. (y) Colocalization scatter plots for MNE-AIEdots in cells at different collection channels and the displayed Pearson's correlation coefficient. (i) NIR-1 channel & NIR-2 channel, (ii) NIR-1 channel & green channel, and (iii) NIR-2 channel & green channel.

cytotoxicity of PFdots, Sqdots, and PcSidots was first assessed with standard MTT assays. The results demonstrated that all of the above-referred nanodots displayed acceptable cytotoxicity to HeLa cells and low photosensitized singlet oxygen generation efficiency (Fig. S26 and S27†), which facilitated further fluorescence imaging applications in living cells. For the cellular imaging study, HeLa cells were incubated with the prepared AIEdots to guarantee the uptake of the nanoparticles. Subsequently, the luminescence signal collected from different optical channels was realized by using different narrow bandpass filters assembled on a multichannel fluorescence microscope with the identical excitation of a xenon lamp (500SP). As shown in Fig. 3, AIEdots were mainly located in the perinuclear regions and presented in the form of bright spots, which was in agreement with the endosomal entry pathway of organic nanoparticles as supported in previous reports.[16,19,27,52–54] In addition, obvious crosstalk in different channels has been observed in cells incubated with TPEdots and TPAdots (Fig. 3a–j). The PFdot and SQdot labeled cells were observed only in their corresponding green and NIR-1 channels. It confirmed that minimal crosstalk interference was obtained when using NE-AIEdots as labels (Fig. 3k–t). Considering the observed high contrast between the perinuclear regions and the rest of the cells, such recognizable fluorescence images of different NE-AIEdots in different channels suggested minimal leakage of the narrow emissive dyes in NE-AIEdots during the process of cell incubation (Fig. S28†).

Taking advantage of the carboxyl group on the surface of NE-AIEdots, functionalized bioconjugation with streptavidin and DNA was performed by EDC-catalyzed coupling. According to the results of gel electrophoresis measurement (Fig. S29†), streptavidin-modified PFdots (PFdots-SA) and DNA-modified SQdots (SQdots-DNA) showed obviously decreased mobility in the gel, as compared to bare NE-AIEdots. These results confirmed that successful linkage between biomolecules and NE-AIEdots was realized. DLS and TEM measurements showed that the modified NE-AIEdots had a slightly increased size compared to the corresponding bare NE-AIEdots (Fig. S30†). Subsequently, the cellular fluorescence imaging of PFdots-SA and SQdots-DNA was further studied. As shown in Fig. S31 and S32,† the modified PFdots-SA, and SQdots-DNA were evenly distributed in the cytoplasm, which was significantly different from their corresponding bare NE-AIEdots. These results might be attributed to the physiological activity of conjugated biomolecules, which could alter the pathway of AIEdots into cells. Additionally, taking advantage of the nanoprecipitation method, multiple emissive AIEdots (MNE-AIEdots) featuring triple narrow emission bands were obtained by assembling the corresponding polymers, including TPE-BT, PFBDP, SQ, PcSi, and PS-PEGCOOH. As illustrated in Fig. 3u–y, MNE-AIEdots exhibited completely distinguishable emissions in three channels corresponding to PFBDP, SQ, and PcSi components, respectively (Fig. S33†). This result indicated that the method presented here could be used as a promising barcode strategy to design fluorescence probes for multiplexed labeling and imaging.

Intraoperative identification of lymph nodes in tumor resection surgery was of great importance to the precise treatment of cancer.[55,56] Fluorescence imaging is considered to be a convenient and noninvasive approach for *in vivo* imaging of lymph nodes. Numerous luminescent probes, especially luminescent nanoprobes are widely used for fluorescence imaging of lymph nodes *in vivo*.[57–63] To further reveal the imaging capabilities of the as-fabricated probes *in vivo*, NE-AIEdots were then applied in multiplexed lymphography. PFdots, SQdots, PcSidots, and MNE-AIEdots were separately administered by subcutaneous injection (0.5 mg mL^{-1}, 25 μL) on footpads of nude mice (Fig. 4a). The *in vivo* fluorescence imaging was monitored and recorded using an EMCCD camera under the excitation of a 450 nm LED lamp and the fluorescence signal was separately collected through 495LP, 550BP, 732BP, and 792BP filters. As shown in Fig. 4b, after injection of the prepared NE-AIEdots and MNE-AIEdots for 0.5 h, strong fluorescence signals were observed at all of the injection sites on the legs. Furthermore, according to the fluorescence image of dissected mice, the injected AIEdots were successfully enriched in the lymph node tissues. The distribution of each kind of NE-AIEdots at different positions could be discriminated from the view of the three channels with

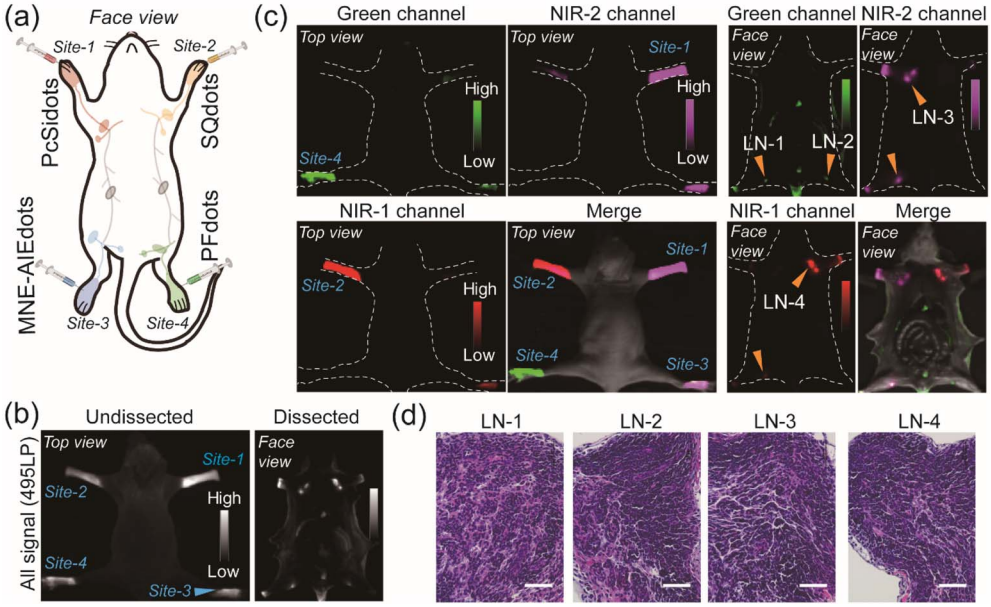

Fig. 4 (a) Schematic illustration of the design for the multicolor fluorescence imaging *in vivo* by using NE-AIEdots and MNE-AIEdots. (b) Fluorescence images of mice under a collection condition in the all signal channels (495LP). (c) Fluorescence images of mice under different collection conditions: green channel (495LP), NIR-1 channel (732BP), and NIR-2 channel (792BP), respectively. The merged channel corresponded to the overlay of the fluorescence images collected from different collection channels and the brightfield image. Excitation: 450 nm. Exposure time: 10 ms. (d) H&E staining images of the lymph node tissues that were detected in (c). Scale bar: 50 μm.

a bandpass filter (Fig. 4c). Distinguishable fluorescence signals could be observed from the legs injected with NE-AIEdots, which separately belonged to the emission of PFdots, Sqdots, and PcSidots, as visualized in single-channel images. Additionally, obvious fluorescence signals were observed in all three different fluorescence channels for MNE-AIEdots, which was in accordance with the multiple emission bands of MNE-AIEdots. Thus, multicolor fluorescence imaging *in vivo* has been successfully realized by using the as-designed NE-AIEdots under a single excitation light source. Then, multicolor fluorescence imaging of the lymph nodes was investigated by using the above-developed NE-AIEdots. According to the guidance of fluorescence imaging, the lymph nodes that displayed distinguishable colors were successfully resected from the mice. The excised lymph node tissues were further analyzed by H&E analysis (Fig. 4d). These results indicated that the ultra-bright NE-AIEdots were prospective candidates for stable and reliable multiplexed fluorescence imaging and detection *in vivo*.

Conclusions

In summary, using the concept of a light-harvesting nanosystem with AIEdots as a light-harvesting antenna and a narrow emissive fluorophore as an emitter, a type of quantum dot-sized organic fluorescent nanoprobe termed NE-AIEdots were successfully synthesized. They had narrow emission bandwidth, tunable emission wavelength, high brightness, and a large Stokes shift. The emission FWHM values of these NE-AIEdots varied from 18 nm to 36 nm, which were 3–6.3 times narrower than conventional AIEdots. Single-particle brightness evaluation indicated that PFdots were about 5.2 times brighter than commercial QD525 under identical excitation conditions, while NIR emissive SQdots had a comparative brightness with QD625. Successful bioconjugation of NE-AIEdots could also easily be realized, helping the nanoparticles enter cells and providing a direct research basis for future targeting-related imaging applications. Multichannel cellular fluorescence imaging of NE-AIEdots with a single emission band and encodable MNE-AIEdots with triple emission bands suggested that these bright narrow emissive AIEdots were promising candidates for multiplexed cell labeling and barcoding applications. Furthermore, by using PFdots, SQdots, PcSidots, and MNE-AIEdots, multiplexed fluorescence imaging of lymph nodes in living mice was realized, which supported the future applications of NE-AIEdots for *in vivo* multiplexed labeling and clinical surgery.

Ethical statement

Animal experiments were conducted according to the guidelines of the Institutional Animal Care and Use Committee, Laboratory Animal Center, Nantong University.

Data availability

The datasets supporting this article have been uploaded as part of the ESI.†

Author contributions

X. Z., Y. Q., and L. W. devised the method and conceived the project. X. Z. and L. Z. designed and performed the experiments, and analyzed the data. K. Z., S. Li. and X. K. performed the chemical experiments. C. Y. and G. L. performed the biological experiments. Q. W., H. J., M. W., and J. L. contributed to the design of the experiments. All authors contributed to writing the manuscript. All authors have given approval to the final version of the manuscript.

Conflicts of interest

There are no conflicts to declare.

Acknowledgements

The authors thank the National Natural Science Foundation of China (62005132, 31901045, 31901056, and 32171452), Jiangsu Specially-Appointed Professor (06200048 and 06200053), Natural Science Research Project of Higher Education in Jiangsu Province (20KJB150040) and Innovative and Entrepreneurial Research Program in Jiangsu Province for financial support.

Notes and references

1 K. M. Dean and A. E. Palmer, *Nat. Chem. Biol.*, 2014, **10**, 512–523.
2 S. P. Perfetto, P. K. Chattopadhyay and M. Roederer, *Nat. Rev. Immunol.*, 2004, **4**, 648–655.
3 Z. Yang, A. Sharma, J. Qi, X. Peng, D. Y. Lee, R. Hu, D. Lin, J. Qu and J. S. Kim, *Chem. Soc. Rev.*, 2016, **45**, 4651–4667.
4 R. R. Zhang, A. B. Schroeder, J. J. Grudzinski, E. L. Rosenthal, J. M. Warram, A. N. Pinchuk, K. W. Eliceiri, J. S. Kuo and J. P. Weichert, *Nat. Rev. Clin. Oncol.*, 2017, **14**, 347–364.
5 K. D. Wegner and N. Hildebrandt, *Chem. Soc. Rev.*, 2015, **44**, 4792–4834.
6 J. Zhou, Q. Liu, W. Feng, Y. Sun and F. Li, *Chem. Rev.*, 2015, **115**, 395–465.
7 M. Yu, J. Xu and J. Zheng, *Angew. Chem., Int. Ed.*, 2019, **58**, 4112–4128.
8 S. Choi, R. M. Dickson and J. Yu, *Chem. Soc. Rev.*, 2012, **41**, 1867–1891.
9 G. Hong, S. Diao, A. L. Antaris and H. Dai, *Chem. Rev.*, 2015, **115**, 10816–10906.
10 C. Wu and D. T. Chiu, *Angew. Chem., Int. Ed.*, 2013, **52**, 3086–3109.
11 W. Sun, S. Guo, C. Hu, J. Fan and X. Peng, *Chem. Rev.*, 2016, **116**, 7768–7817.
12 N. Boens, V. Leen and W. Dehaen, *Chem. Soc. Rev.*, 2012, **41**, 1130–1172.
13 J. Mei, N. L. Leung, R. T. Kwok, J. W. Lam and B. Z. Tang, *Chem. Rev.*, 2015, **115**, 11718–11940.
14 S. Liu, C. Chen, Y. Li, H. Zhang, J. Liu, R. Wang, S. T. H. Wong, J. W. Y. Lam, D. Ding and B. Z. Tang, *Adv. Funct. Mater.*, 2019, **30**, 1908125.
15 P. Reineck and B. C. Gibson, *Adv. Opt. Mater.*, 2017, **5**, 1600446.
16 A. Reisch and A. S. Klymchenko, *Small*, 2016, **12**, 1968–1992.
17 Z. Tian, A. D. Shaller and A. D. Li, *Chem. Commun.*, 2009, 180–182.
18 O. S. Wolfbeis, *Chem. Soc. Rev.*, 2015, **44**, 4743–4768.
19 W. R. Algar, M. Massey, K. Rees, R. Higgins, K. D. Krause, G. H. Darwish, W. J. Peveler, Z. Xiao, H. Y. Tsai, R. Gupta, K. Lix, M. V. Tran and H. Kim, *Chem. Rev.*, 2021, **121**, 9243–9358.
20 E.-B. Cho, D. O. Volkov and I. Sokolov, *Adv. Funct. Mater.*, 2011, **21**, 3129–3135.
21 N. Melnychuk, S. Egloff, A. Runser, A. Reisch and A. S. Klymchenko, *Angew. Chem., Int. Ed.*, 2020, **59**, 6811–6818.
22 K. Trofymchuk, A. Reisch, P. Didier, F. Fras, P. Gilliot, Y. Mely and A. S. Klymchenko, *Nat. Photon.*, 2017, **11**, 657–663.
23 N. Melnychuk and A. S. Klymchenko, *J. Am. Chem. Soc.*, 2018, **140**, 10856–10865.
24 J. Chen, S. M. A. Fateminia, L. Kacenauskaite, N. Baerentsen, S. Gronfeldt Stenspil, J. Bredehoeft, K. L. Martinez, A. H. Flood and B. W. Laursen, *Angew. Chem., Int. Ed.*, 2021, **60**, 9450–9458.
25 S. Xu, Y. Duan and B. Liu, *Adv. Mater.*, 2020, **32**, e1903530.
26 K. Li, Z. Zhu, P. Cai, R. Liu, N. Tomczak, D. Ding, J. Liu, W. Qin, Z. Zhao, Y. Hu, X. Chen, B. Z. Tang and B. Liu, *Chem. Mater.*, 2013, **25**, 4181–4187.
27 G. Feng, C. Y. Tay, Q. X. Chui, R. Liu, N. Tomczak, J. Liu, B. Z. Tang, D. T. Leong and B. Liu, *Biomaterials*, 2014, **35**, 8669–8677.
28 X. Zhu, J. X. Wang, L. Y. Niu and Q. Z. Yang, *Chem. Mater.*, 2019, **31**, 3573–3581.
29 H. Fujioka, J. Shou, R. Kojima, Y. Urano, Y. Ozeki and M. Kamiya, *J. Am. Chem. Soc.*, 2020, **142**, 20701–20707.
30 J. E. Jeong, M. A. Uddin, H. S. Ryu, H. C. Kim, M. Kang, J. F. Joung, S. Park, S. H. Shim and H. Y. Woo, *Chem. Mater.*, 2020, **32**, 6685–6696.
31 Z. Zhao, C. Chen, S. Wei, H. Xiong, F. Hu, Y. Miao, T. Jin and W. Min, *Nat. Commun.*, 2021, **12**, 1305.
32 C. Chen, B. Corry, L. Huang and N. Hildebrandt, *J. Am. Chem. Soc.*, 2019, **141**, 11123–11141.
33 Y. Rong, C. Wu, J. Yu, X. Zhang, F. Ye, M. Zeigler, M. E. Gallina, I. C. Wu, Y. Zhang, Y. H. Chan, W. Sun, K. Uvdal and D. T. Chiu, *ACS Nano*, 2013, **7**, 376–384.
34 M. Panagiotopoulou, Y. Salinas, S. Beyazit, S. Kunath, L. Duma, E. Prost, A. G. Mayes, M. Resmini, B. Tse Sum Bui and K. Haupt, *Angew. Chem., Int. Ed.*, 2016, **55**, 8244–8248.
35 C. S. Ke, C. C. Fang, J. Y. Yan, P. J. Tseng, J. R. Pyle, C. P. Chen, S. Y. Lin, J. Chen, X. Zhang and Y. H. Chan, *ACS Nano*, 2017, **11**, 3166–3177.
36 Y. Fan, P. Wang, Y. Lu, R. Wang, L. Zhou, X. Zheng, X. Li, J. A. Piper and F. Zhang, *Nat. Nanotechnol.*, 2018, **13**, 941–946.

37 I. C. Wu, J. Yu, F. Ye, Y. Rong, M. E. Gallina, B. S. Fujimoto, Y. Zhang, Y. H. Chan, W. Sun, X. H. Zhou, C. Wu and D. T. Chiu, *J. Am. Chem. Soc.*, 2015, **137**, 173–178.
38 C. Wu, T. Schneider, M. Zeigler, J. Yu, P. G. Schiro, D. R. Burnham, J. D. McNeill and D. T. Chiu, *J. Am. Chem. Soc.*, 2010, **132**, 15410–15417.
39 M. H. Liu, Z. Zhang, Y. C. Yang and Y. H. Chan, *Angew. Chem., Int. Ed.*, 2021, **60**, 983–989.
40 L. Chen, D. Chen, Y. Jiang, J. Zhang, J. Yu, C. C. DuFort, S. R. Hingorani, X. Zhang, C. Wu and D. T. Chiu, *Angew. Chem., Int. Ed.*, 2019, **58**, 7008–7012.
41 D. Ding, C. C. Goh, G. Feng, Z. Zhao, J. Liu, R. Liu, N. Tomczak, J. Geng, B. Z. Tang, L. G. Ng and B. Liu, *Adv. Mater.*, 2013, **25**, 6083–6088.
42 S. Liu, H. Zhang, Y. Li, J. Liu, L. Du, M. Chen, R. T. K. Kwok, J. W. Y. Lam, D. L. Phillips and B. Z. Tang, *Angew. Chem., Int. Ed.*, 2018, **57**, 15189–15193.
43 O. Galangau, C. Dumas-Verdes, R. Meallet-Renault and G. Clavier, *Org. Biomol. Chem.*, 2010, **8**, 4546–4553.
44 U. Mayerhoffer, B. Fimmel and F. Wurthner, *Angew. Chem., Int. Ed.*, 2012, **51**, 164–167.
45 J. Mei, Y. Hong, J. W. Y. Lam, A. Qin, Y. Tang and B. Z. Tang, *Adv. Mater.*, 2014, **26**, 5429–5479.
46 K. Li, W. Qin, D. Ding, N. Tomczak, J. Geng, R. Liu, J. Liu, X. Zhang, H. Liu, B. Liu and B. Z. Tang, *Sci. Rep.*, 2013, **3**, 1150.
47 D. Ding, C. C. Goh, G. Feng, Z. Zhao, J. Liu, R. Liu, N. Tomczak, J. Geng, B. Z. Tang, L. G. Ng and B. Liu, *Adv. Mater.*, 2013, **25**, 6083–6088.
48 D. Zhong, W. Chen, Z. Xia, R. Hu, Y. Qi, B. Zhou, W. Li, J. He, Z. Wang, Z. Zhao, D. Ding, M. Tian, B. Z. Tang and M. Zhou, *Nat. Commun.*, 2021, **12**, 6485.
49 G. Feng, C. Y. Tay, Q. X. Chui, R. Liu, N. Tomczak, J. Liu, B. Z. Tang, D. T. Leong and B. Liu, *Biomaterials*, 2014, **35**, 8669–8677.
50 S. Liu, H. Zhang, Y. Li, J. Liu, L. Du, M. Chen, R. T. K. Kwok, J. W. Y. Lam, D. L. Phillips and B. Z. Tang, *Angew. Chem., Int. Ed.*, 2018, **57**, 15189–15193.
51 Y. Jin, F. Ye, M. Zeigler, C. Wu and D. T. Chiu, *ACS Nano*, 2011, **5**, 1468–1475.
52 B. Andreiuk, A. Reisch, M. Lindecker, G. Follain, N. Peyrieras, J. G. Goetz and A. S. Klymchenko, *Small*, 2017, **13**, 1701582.
53 L. P. Fernando, P. K. Kandel, J. Yu, J. McNeill, P. C. Ackroyd and K. A. Christensen, *Biomacromolecules*, 2010, **11**, 2675–2682.
54 H. S. Peng and D. T. Chiu, *Chem. Soc. Rev.*, 2015, **44**, 4699–4722.
55 G. A. Porter, M. I. Ross, R. S. Berman, W. E. Sumner, J. E. Lee, P. F. Mansfield and J. E. Gershenwald, *Surgery*, 2000, **128**, 306–311.
56 P. Schrenk, W. Rehberger, A. Shamiyeh and W. Wayand, *J. Surg. Oncol.*, 2002, **80**, 130–136.
57 G. Niu and X. Chen, *Theranostics*, 2015, **5**, 686–697.
58 Z. Yang, R. Tian, J. Wu, Q. Fan, B. C. Yung, G. Niu, O. Jacobson, Z. Wang, G. Liu, G. Yu, W. Huang, J. Song and X. Chen, *ACS Nano*, 2017, **11**, 4247–4255.
59 S. Kim, Y. T. Lim, E. G. Soltesz, A. M. De Grand, J. Lee, A. Nakayama, J. A. Parker, T. Mihaljevic, R. G. Laurence, D. M. Dor, L. H. Cohn, M. G. Bawendi and J. V. Frangioni, *Nat. Biotechnol.*, 2004, **22**, 93–97.
60 F. W. Cao, Y. X. Guo, Y. Li, S. Y. Tang, Y. D. Yang, H. Yang and L. Q. Xiong, *Adv. Funct. Mater.*, 2018, **28**, 1707174.
61 A. K. Polomska and S. T. Proulx, *Adv. Drug Delivery Rev.*, 2021, **170**, 294–311.
62 S. Qi, X. Wang, K. Chang, W. Shen, G. Yu and J. Du, *J. Nanobiotechnol.*, 2022, **20**, 24.
63 S. Hameed, H. Chen, M. Irfan, S. Z. Bajwa, W. S. Khan, S. M. Baig and Z. Dai, *Bioconjugate Chem.*, 2019, **30**, 13–28.